Minerals **2014**, *4*, 74-88; doi:10.3390/min4010074

OPEN ACCESS

minerals

ISSN 2075-163X
www.mdpi.com/journal/minerals

Article

Membrane Vesicles as a Novel Strategy for Shedding Encrusted Cell Surfaces

Paul P. Shao [1], Luis R. Comolli [2] and Rizlan Bernier-Latmani [1,*]

[1] Environmental Microbiology Laboratory, École Polytechnique Fédérale de Lausanne, Lausanne CH-1015, Switzerland; E-Mail: paul.shao@epfl.ch

[2] Life Sciences Division, Lawrence Berkeley National Laboratory, Berkeley, CA 94720, USA; E-Mail: lrcomolli@lbl.gov

* Author to whom correspondence should be addressed; E-Mail: rizlan.bernier-latmani@epfl.ch; Tel.: +41-21-693-5001; Fax: +41-21-693-6205.

Received: 10 December 2013; in revised form: 24 January 2014 / Accepted: 27 January 2014 / Published: 7 February 2014

Abstract: Surface encrustation by minerals, which impedes cellular metabolism, is a potential hazard for microbes. The reduction of U(VI) to U(IV) by *Shewanella oneidensis* strain MR-1 leads to the precipitation of the mineral uraninite, as well as a non-crystalline U(IV) product. The wild-type (WT) strain can produce extracellular polymeric substances (EPS), prompting precipitation of U some distance from the cells and precluding encrustation. Using cryo-transmission electron microscopy and scanning transmission X-ray microscopy we show that, in the biofilm-deficient mutant Δ*mxd*A, as well as in the WT strain to a lesser extent, we observe the formation of membrane vesicles (MVs) as an additional means to lessen encrustation. Additionally, under conditions in which the WT does not produce EPS, formation of MVs was the only observed mechanism to mitigate cell encrustation. Viability studies comparing U-free controls to cells exposed to U showed a decrease in the number of viable cells in conditions where MVs alone are detected, yet no loss of viability when cells produce both EPS and MVs. We conclude that MV formation is a microbial strategy to shed encrusted cell surfaces but is less effective at maintaining cell viability than the precipitation of U on EPS.

Keywords: biomineralization; uranium; detoxification; cryo-microscopy; spectro-microscopy

---

1. Introduction

Microbes living in an environment containing metals are exposed to biotic and abiotic reactions that can result in nucleation of minerals on their outer surface [1,2]. Excessive mineral formation on the cell surface can lead to complete cell encrustation, potentially impeding cellular metabolism and limiting the microbe's capacity to interface with its environment. Nonetheless, certain microbes are intricately involved in iron [3–5] and manganese [6,7] oxidation, as well as the reduction of a variety of metals and metalloids, all of which lead to mineral formation [8]. How cellular encrustation is avoided or mitigated is not well characterized, but it is vital to complete our understanding of microbial metal cycling.

A number of mechanisms to minimize encrustation have been identified primarily for Fe(II)-oxidizing bacteria [9] and include the localization of metal sorption or precipitation on extracellular structures some distance for the cells [2,10], the solubilization of minerals by modifying the pH microenvironment around the cell [2,11], and/or altering surface charge properties [12,13]. These microorganisms are likely to employ a combination of these strategies to prevent encrustation.

In contrast, there is no clear mechanism for preventing membrane encrustation in metal-reducing microorganisms reducing U, such as *Shewanella oneidensis* strain MR-1 or *Geobacter sulfurreducens* [14,15].

Here, we use a model system whereby *S. oneidensis* can be induced to sequester hexavalent uranium [U(VI)] as a result of reduction to tetravalent uranium [U(IV)] [16]. Depending on the chemical composition of the medium used, the immobilized U product can be either a non-crystalline U(IV) species associated with phosphate groups on biomass [17,18], or a biogenic uraninite (bio-UO_2) species that is compositionally approximately 50% crystalline UO_2 [a nanocrystalline U(IV) oxide] and 50% non-crystalline U(IV) [16,19]. Previous work has shown that in the case of non-crystalline U(IV), a biological response to U occurs, triggering the production of extracellular polymeric substances (EPS). EPS modulates the U product and has a protective effect on cellular viability by allowing the accumulation of U some distance from the cell [20]. In contrast, where bio-UO_2 is produced, U product precipitates primarily on the cell surface and can lead to complete cell encrustation, resulting in a loss of cellular viability [20].

Membrane vesicles (MVs) originating from Gram-negative bacteria are spherical structures compositionally similar to the outer membrane from which they are formed [21,22]. As MVs form blebs through increased positive curvature of the outer membrane, they encapsulate the periplasm so that once released, they become independent membrane-bound vessels capable of delivering periplasmic contents [23]. MVs have been implicated in a myriad of biological roles [21]. Offensively, MVs can be used to deliver and disseminate bacterial products to the environment. Examples include delivery of adhesin proteins [24,25], hydrolytic enzymes [26–29], quorum-signaling molecules [30,31], and genetic material [32,33]. Defensively, MVs can be used to promote bacterial survival. They are found as components of biofilm matrices [34,35], can export unwanted host immune response and antibiotics [36,37], and are generated as a response to envelope stress [38]. Mineralized vesicles have also been identified in a number of environments from hot springs [39], in acid mine drainage [40], and in the laboratory [41].

In this work, we examined the role of MVs in shedding biomineralized outer membranes and preserving cell viability through the elimination of cell encrustation. We used cryogenic transmission electron microscopy (cryo-TEM) and scanning transmission X-ray microscopy (STXM) to investigate the formation of MVs in wild-type cells producing either bio-UO_2 or non-crystalline U(IV), as well as in an EPS-impaired *S. oneidensis* mutant, Δ*mxd*A. Our results show that MV formation benefits the cells to some extent for the preservation of viability in cells challenged with U. MV formation occurred in all the above conditions, but varied in the degree of abundance of the MV. Hence, we conclude that membrane vesicle formation in *S. oneidensis* is a novel strategy for shedding encrusted cell surfaces.

2. Results and Discussion

2.1. Results

2.1.1. U Associated with Both EPS and MV in Wild-Type Strain MR-1 Producing Non-Crystalline U(IV)

The association of U with the outer membrane and with extracellular material is evident in the case where non-crystalline U(IV) is produced (Figure 1). U(IV) product speciation was confirmed (Figure 2) as primarily non-crystalline U(IV) by a chemical extraction technique developed in our laboratory [19]. At low U(VI) loadings or in the early stages of U reduction, cells display a discrete distribution of U(IV) on their surfaces, suggesting localized reduction of U(VI) (Figure 1a). Previous studies show that U accumulates primarily extracellularly, in large swaths of lipid and polysaccharide-rich extracellular polymeric substances (EPS) [16,20]. Here, we show that in addition to EPS localization (Figure 1c,d), U accumulates on the outer membrane and on membrane vesicles (Figure 1a,b). In Figure 1a, MVs (indicated by arrows) are embedded in abundant hair-like, electron dense material corresponding to U(IV). Similarly, in Figure 1b, MVs are observed away from the cell in loose association with electron dense material. In contrast, strain MR-1 cells not exposed to U do not exhibit EPS or MV formation (Figure 3). These cryo-TEM images suggest that U(VI) reduction results in the accumulation of U(IV) in association with the cell membrane as well as by the production of MVs that remove U from the cell surface and EPS onto which U(IV) accumulates.

Cryo-TEM of intact cells offered the best images of U association to EPS and MVs as 2D projections (Figure 1a). Moreover, cryo-sectioned samples via cryo-electron microscopy of vitreous ice sections (CEMOVIS) predominantly showed U associated with fibrillar branches extracellular to cells that appear slightly deformed (Figure 1c,d). It is likely that the fibrils observed in these sections have contributions from EPS-associated and MV-associated U product, but are indistinguishable due to limited *z*-direction information. Additionally, cell viability appeared unaffected by the presence of U under these conditions (Figure 4).

Figure 1. *S. oneidensis* MR-1 producing non-crystalline U(IV). (**a**) and (**b**) Cryogenic transmission electron microscopy (cryo-TEM) images of intact flash-frozen cell suspensions. (**a**) Cells producing electron dense U "tufts" associated with extracellular polymeric substances (EPS). MVs are most prominently observed embedded in the electron-dense U mass on the right side (blue arrows). (**b**) Cell producing larger-sized membrane vesicles (MVs). Electron-dense U is observed as smaller fibrils. (**c**) and (**d**) Cryo-electron microscopy of vitreous ice sections (CEMOVIS) images showing fibrillar non-crystalline U(IV) protruding from the sectioned cell surface and associated with EPS.

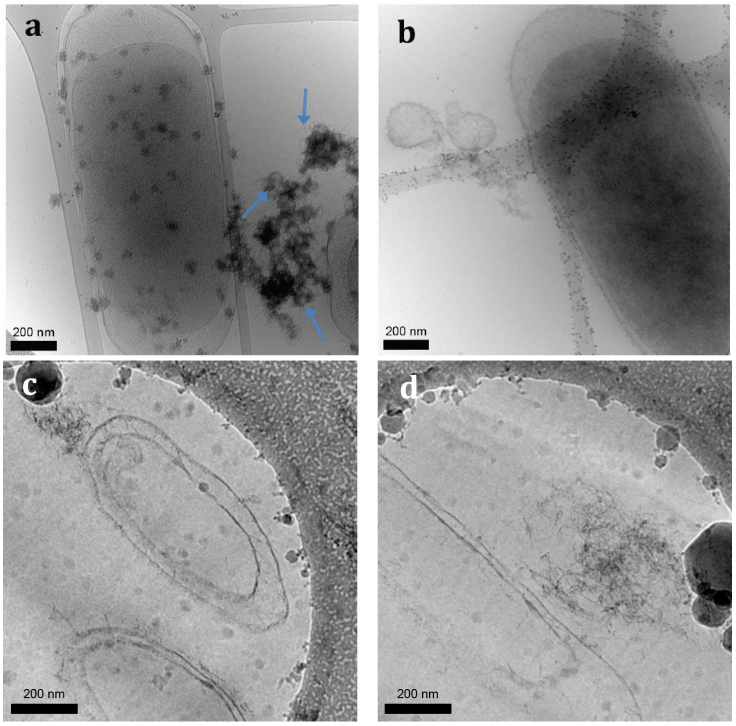

Figure 2. Wet chemical extraction. Based on [19], this method can be used to determine the contribution of non-crystalline U(IV) to the total U(IV). By subtraction, the contribution of UO_2 can be inferred. MR-1 WT and Δ*mxd*A in WLP conditions produce primarily non-crystalline U(IV), as evidenced by the extraction of the majority of U(IV) present in this system. In contrast, MR-1 BP produces bio-UO_2, which is about 50% non-crystalline U(IV) and 50% uraninite, as is reflected in the recovery of ~55% of the total U(IV) by extraction.

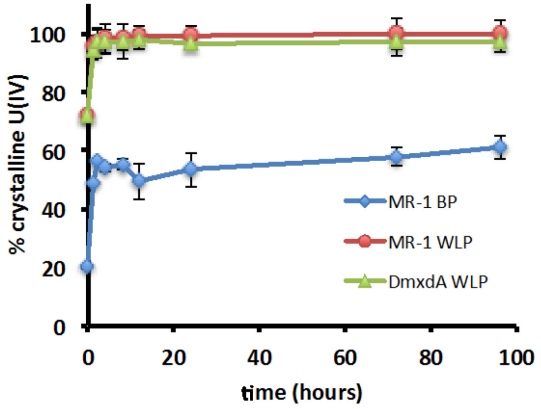

Figure 3. *S. oneidensis* MR-1 in the absence of U reduction. (**a**) Cryo-TEM image of intact flash-frozen cell. Crystalline ice formation due to imperfect freezing accounts for the electron dense spots observed on and around the cell. (**b**) CEMOVIS image. Examples of sectioned cells are outlined in orange. MVs were not observed in either cryo preparation in the absence of U.

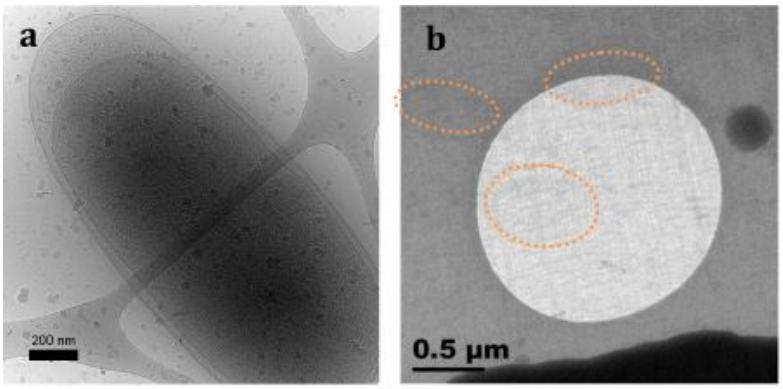

Figure 4. Viability studies. Due to the non-growth conditions, there is an inherent decrease in cell viability over time. Relative viability in the presence *versus* absence of U at 24 h is a rough metric of the impact of U reduction. Strain MR-1 producing uraninite (bio-UO_2) suffers more than a magnitude decrease in cell viability. Whereas cell viability of MR-1 producing non-crystalline U(IV) is roughly equivalent with and without U. Δ*mxd*A mutant producing non-crystalline U(IV) suffers loss of cellular viability to a lesser extent that the wild-type (WT) strain producing bio-UO_2 but more than WT strain producing non-crystalline U(IV). The data marked with an asterisk indicates that the difference between the treatments is significant based on a student's t test with a confidence interval of 0.05.

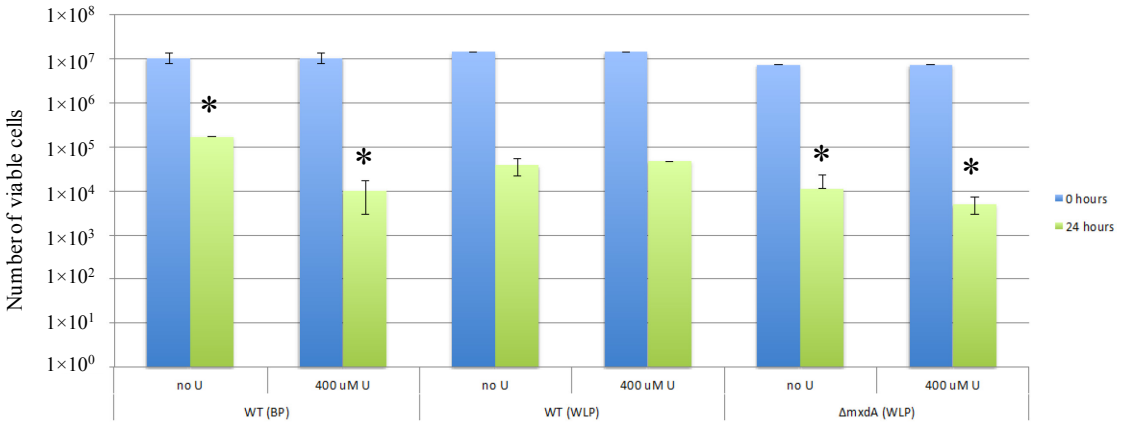

2.1.2. Extensive MV Generation in Biofilm-Deficient Mutant (Δ*mxd*A) Producing Non-Crystalline U(IV)

EPS production was shown to be important in mitigating U toxicity [20]. The *S. oneidensis* deletion mutant strain Δ*mxd*A, in which the gene encoding for cyclic-di-GMP production is knocked out, is characterized by a loss of biofilm stability [42,43]. Hence, we probed the formation of EPS and MV in this mutant strain. Cell aggregates were imaged using scanning transmission X-ray microscopy (STXM), a method that enables mapping of biomolecules (proteins, lipids, polysaccharides) based on

their carbon K-edge X-ray absorption spectra. Tri-color maps representing the biomolecules show that EPS consisted of mostly polysaccharide structured into an amorphous pool encompassing several cells (Figure 5a). Uranium, primarily in the form of non-crystalline U(IV) (Figure 2), co-localized with the cell bodies, not with the polysaccharide-rich and lipid-poor EPS (Figure 5b). This was in stark contrast to U challenged wild-type (WT) cells that produced U co-localized with EPS consisting of a fibrillar lipid/polysaccharide network (Figure S1) [20]. Most strikingly, when intact cells were observed by cryo-TEM, Δ*mxd*A produced copious amounts of MVs. U was observed associated with both the cell and the MVs (Figure 5c,d). The cells appear to be significantly covered with U and, at the same time, numerous U-coated MVs are shed from the cell surface. Cell encrustation is apparent but not extensive and, as a result, it is still possible to visualize entire cells in cryo-transmission mode. Hence, U(IV) appears to associated with the cell membrane as well as MVs released from the cell. Cell viability was impacted by the presence of U under these conditions to a greater extent than for strain MR-1 under conditions producing non-crystalline U(IV) (Figure 4).

Figure 5. *S. oneidensis* Δ*mxd*A biofilm-deficient mutant producing non-crystalline U(IV). (**a**) Scanning transmission X-ray microscopy (STXM) carbon speciation represented by red-green-blue tri-color map. Protein is shown in red, lipid in green, and polysaccharide in blue. (**b**) STXM uranium map of the same region. Orange dotted line marks EPS boundary and the location of cell bodies. (**c**) and (**d**) Cryo-TEM images of intact cells producing extensive MVs coated with electron-dense U.

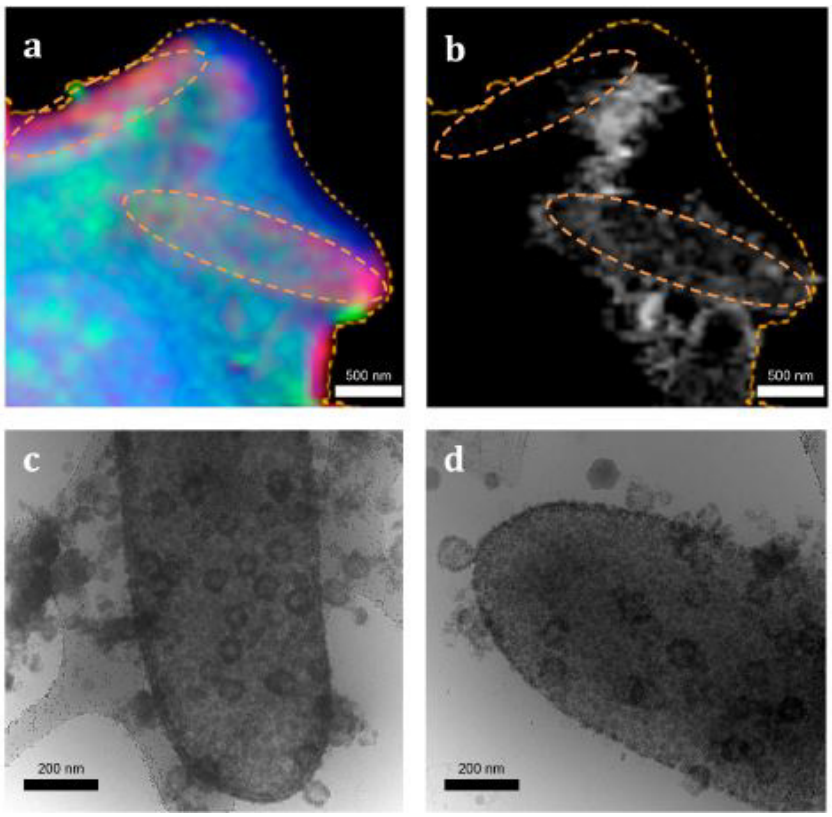

2.1.3. Limited MV Production of Wild-Type Strain MR-1 Producing Bio-UO_2 despite Severe Encrustation

In the case where strain MR-1 produces bio-UO_2 (Figure 6), U was shown to accumulate primarily on the cell surface [16,20] and this is exemplified by the heavy encrustation of the cells whereby electron dense U completely surrounds the cell and has potentially permeated into the periplasmic space, as evidenced in CEMOVIS images (Figure 6b,c). No such encrustation is visible in cryo-TEM performed on intact cells due to the inability of the beam to penetrate through such regions and, thus, the selective exclusion of those cells from imaging. However, in lightly U-impacted cells, the presence of occasional MVs was visualized in association with whole cells (Figure 6d,e). Additionally, on a single occasion, MV formation was visualized in a cryo-section (Figure 6c). Finally, in some instances, electron dense U product was observed distant from the cell (Figure 6f). While MVs were evidenced in these samples, by far the most common phenotypes observed by CEMOVIS were either discrete accumulations of UO_2 nanoparticles on the cell outer membrane or heavy encrustation of the outer membrane and, in some cases, the periplasmic space. In contrast to the two cases above, cell viability was severely inhibited in the presence of U (Figure 4). There was approximately an order of magnitude decrease in viability in the case where U was present.

Figure 6. *S. oneidensis* MR-1 producing biogenic uraninite. (**a**) CEMOVIS image showing biogenic uraninite nucleation on the cell surface. (**b**) CEMOVIS image showing a cell fully encrusted by U. (**c**) CEMOVIS image of a fully encrusted cell budding a vesicle. (**d**) and (**e**) Cryo-TEM images of cells producing MVs. Electron-dense U can be seen associated with the MVs and scattered across the cell. These correspond to the nucleating morphology seen in CEMOVIS. (**f**) MVs and biogenic uraninite distant from the cell. One large MV is prominently visible. Additional smaller MVs are observed amidst the electron-dense U.

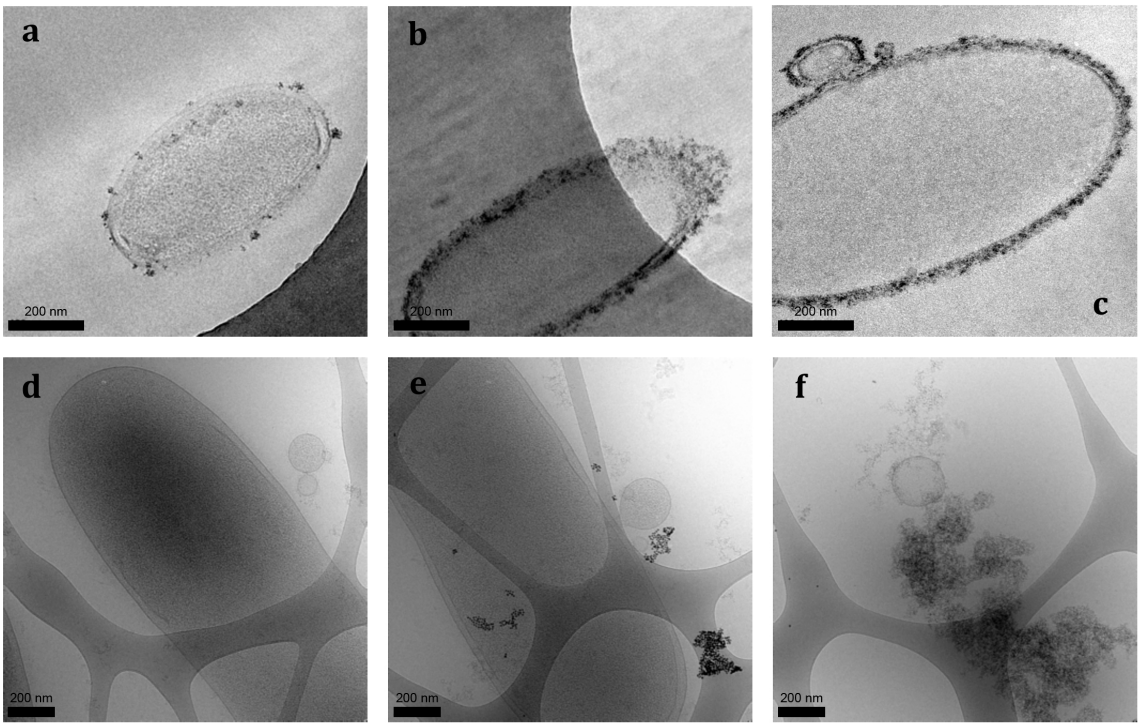

2.2. Discussion

In this work, we found a clear correlation between MV formation and exposure to U in *S. oneidensis* strain MR-1. In cells incubated in the absence of U, no evidence for MV formation was uncovered (Figure 3), while in cells exposed to U, the contribution of MVs (although variable depending on the treatment) was always noticeable (Figures 1, 5 and 6). As was reported for *Shewanella* sp. strain CN32 and *Shewanella* sp. strain MR-1 [44], the MVs produced are derived from blebs of the outer membrane and appear to be composed of a single bilayer corresponding to the outer membrane. The MVs vary in size from 50 nm to ~200 nm.

A previous study of MVs in *Shewanella* spp. has suggested their role in directly catalyzing metal reduction and precipitation but the specific mechanism triggering their release was not identified [44]. The authors speculated the possible function of freeing cells of Fe(II) accumulated during iron respiration but were unable to substantiate the claim.

In this work, we show that an additional role of membrane vesicles is in shedding parts of the membrane that are mineral-encrusted as a result of metal reduction. The cells have a mechanism for shedding outer membrane encrusted with U by blebbing off those portions of the membrane through the formation of vesicles. MV formation was observed in all three conditions considered: WT producing either non-crystalline U(IV) or bio-UO_2 as well as mutant Δ*mxd*A producing non-crystalline U(IV). We show that the greatest MV production occurs for the mutant. This is because the mutant is incubated in a medium (WLP, see materials and methods) that supports the synthesis of additional membrane components for MV release. This mutant is deficient in cyclic-di-GMP synthesis, resulting in an altered EPS composition (Figure 5) in comparison to WT [20]. Due to this different EPS composition, U(VI) reduction does not take place primarily in the EPS as for the WT but rather on the cell surface. Thus, we propose that to maintain the viability of the cells (Figure 4) and avoid incrustation, vesicles are produced profusely and allow the removal of surface-accumulated U. The formation of vesicles appears to maintain viability to a greater extent than for cells producing uraninite. It may come as a surprise that non-crystalline U(IV) is formed in this case despite the association of U(IV) with the membrane, which typically leads to bio-UO_2 formation [20]. However, the formation of non-crystalline U(IV) is consistent with the association of U(IV) with phosphate groups on the membrane. We propose the following explanation: as vesicles are formed, additional phosphate functional groups are created on the newly formed membrane, allowing for further non-crystalline U(IV) formation. As long as the MVs are formed and provide additional phosphate functional groups that bind U(IV), UO_2 precipitation is precluded.

In comparison, the WT in the same medium, producing non-crystalline U(IV), generates comparatively fewer MVs. We attribute this difference to the preferential reduction of U(VI) in the EPS rather than on the cell surface [20]. As a result of the limited association of U(IV) with the cell membrane, there is limited need for the formation of MVs and this is reflected by microscopy (Figure 1). As shown in Figure 1a, there is initial U(IV) association with the membrane in the form of tufts but this is quickly overtaken by the association of U with phosphate functional groups in EPS. MVs serve to alleviate toxicity associated with the association—albeit minimal—of U with the cell membrane.

Finally, the case in which WT is producing bio-UO_2 also shows limited MV formation. In this case, acute U toxicity is evidenced (Figure 4). We propose that the medium in this case (composed solely of

$NaHCO_3$ and PIPES buffer) does not support the formation of vesicles due to its paucity in building blocks for the synthesis of membrane components. The cells are in a metabolically precarious state and are not able to produce additional biomolecules. This explanation is supported by the lack of production of EPS in this case. The few MVs produced are not present in sufficient numbers to prevent the massive encrustation of *S. oneidensis* cells (Figure 6). Due to this unavoidable encrustation, cell viability decreases by an order of magnitude (Figure 4).

Hence, MVs serve as a detoxification strategy for *S. oneidensis* cells when the physiological conditions allow for the synthesis of new biomolecules. This strategy appears to complement the production of EPS, that itself prevents U precipitation on the cell body [20]. This is the first time that MVs are implicated in metal detoxification and indeed the first time they are identified during microbial U(VI) reduction. This finding is probably due to the use of cryo-TEM, which allows fixation by flash freezing, preserving the samples intact in a frozen hydrated state. It is well established that cryo fixation is the most effective sample preparation to avoid artifacts originating from chemical fixation and dehydration [45]. We also avoided centrifugation, which has been suggested to artificially generate MVs. Incidentally, it may be possible to identify membrane vesicles using whole cells mounts as we identified MV-like features in an electron microscopy image in a publication investigating U(VI) reduction by pili-deficient *Geobacter sulfurreducens* [46]. The authors did not mention this observation in the text but the presence of MVs is quite evident in the case in which pili-less cells are exposed to U. This observation suggests that MV formation to combat incrustation may not be an exclusive characteristic of *S. oneidensis* and may be more widely distributed among metal reducing bacteria.

The production of membrane vesicles as a detoxification response to U toxicity is consistent with the results of a transcriptomic study considering U(VI) reduction by *S. oneidensis* sp. strain MR-1 [47]. In that study, the genes encoding for a spheroplast protein precursor and various outer membrane proteins were amongst the most upregulated in response to U, leading the authors to suggest membrane damage as a mode of U toxicity. At that time, no information on detoxification strategies was available. However, in retrospect, it is reasonable to assume that the production of membrane vesicles required the synthesis of a variety of outer membrane precursors and their upregulation is consistent with the need for further membrane synthesis.

Previous work has suggested that the surface of *Shewanella* sp. strain CN32 is composed of a heterogeneous distribution of functional groups resulting in non-uniform charge distribution [48]. Additionally, electrostatic force microscopy has shown that negatively charged zone about 50 nm in diameter are distributed on the cell surface corresponding to raised areas [49]. It is tempting to speculate that those areas correspond to the areas of *c*-type cytochrome localization, resulting in U accumulation and, ultimately, to blebs and, then, vesicles release.

3. Experimental Section

3.1. Bacterial Cultures and Uranium Reduction

All reagents in this study were certified analytical grade or higher, and ultrapure water was used to prepare solutions. Culturing and growth of *Shewanella oneidensis* MR-1 was conducted as described

previously [16] and was carried out in the same manner for the Δ*mxd*A mutant [42,43]. This mutant was engineered to knock-out the gene encoding for cyclic-di-GMP production and its main phenotype is a loss of biofilm stability. Hence, biofilm formation is disrupted but EPS production is impacted but not halted. Microbial U(VI) bioreduction was conducted under strict anaerobic conditions. Reactions were carried out inside butyl rubber stoppered serum bottles inside an anoxic chamber with an atmosphere of 2%–5% H_2 and a balance of N_2. Reduction media were filter-sterilized and made anoxic through N_2 purging for several hours and allowed to equilibrate in the anoxic chamber for several days prior to the experiment. Biogenic UO_2 was preferentially produced in an anoxic simple medium (BP) containing 20 mM 1,4-piperazinediethanesulfonic acid (PIPES) buffer set to pH 6.8 and 30 mM sodium bicarbonate. Monomeric U(IV) was preferentially produced in anoxic Widdel low phosphate (WLP) medium [16]. To initiate U(VI) reduction, 20 mM L(+)-lactic acid and 0.4 mM uranyl acetate were added to each cell suspension [19].

3.2. Cryo-Sections (CEMOVIS)

For CEMOVIS, samples were supplemented with 20% dextran (average molecular mass 40 kDa; Sigma-Aldrich, Buchs, Switzerland). They were then introduced into copper tubes and pressure frozen with an EM PACT high-pressure freezer (Leica, Vienna, Austria). Tubes were then mounted in an FC6/UC6 cryo-ultramicrotome (Leica) and trimmed with a cryotrim 45 diamond knife (Diatome, Bienne, Switzerland) to a pyramidal shape as previously described [50]. Sixty-five nanometer feed cryosections were cut with a 35° diamond knife (Diatome). They were collected on Quantifoil 1.2/1.3 grids and stored in liquid nitrogen until imaging. Grids were transferred to a cryoholder (Gatan, Pleasanton, PA, USA) and inserted into a CM12 (FEI, Eindhoven, The Netherlands) equipped with a LaB6 cathode, cryo-transfer stage and imaged with an acceleration voltage of 100 kV. Images were recorded on a Gatan 1 k × 1 k CCD camera (Gatan).

3.3. 2D and 3D Cryo-TEM

For cryo-TEM images and tomographic tilt series, aliquots of 5 μL of sample were loaded onto lacey carbon grids (Cat No. 01881, Ted Pella, Redding, CA, USA) that were pretreated by glow-discharge. The Formvar support was not removed from the lacey carbon. The grids were manually blotted with filter paper and plunged into liquid ethane at near liquid nitrogen temperature using a portable cryo-plunge device [39]. Grids were stored in liquid nitrogen until further analysis. Images were acquired on a JEOL-3100 transmission electron microscope equipped with a FEG electron source operating at 300 kV, an Omega energy filter, a cryo-transfer stage, and a Gatan 795 2 k × 2 k CCD camera (Gatan) mounted at the exit of an electron decelerator held at a voltage of 200 to 250 kV [42]. The stage was cooled with liquid nitrogen to 80 K during acquisition of all data sets. Images were recorded at different magnifications giving a pixel size of 0.375, 0.28, or 0.12 nm at the specimen. Underfocus values ranged between 3.6 ± 0.25 μm to 12 ± 0.5 μm, and energy filter widths were typically around 30 eV. More than 200 images (2D projections) were acquired. The survey of the grids and the selection of suitable targets were done in low dose defocused diffraction mode. Ten tomographic tilt series were acquired under low-dose conditions, typically over an angular range between +65° and −65°, ±5° with increments of 2° and a pixel size of 0.375 nm at the specimen.

Between 62 and 70 images were recorded for each tilt series, acquired semi-automatically with the program Serial-EM [51] adapted to JEOL microscopes. All tomographic reconstructions were obtained with the program Imod [51,52]. The typical doses used per complete tilt series were ~100 to 140 $e^{-}Å^{-2}$. The program ImageJ (NIH, [53]) was used for analysis of the 2D image projections.

3.4. Scanning Transmission X-Ray Microscopy (STXM)

Biomolecules were mapped and co-localized with uranium maps in our sample using STXM stacks at the carbon K-edge and uranium $4d_{5/2}$ edge respectively. Samples were prepared as described previously [20]. Carbon reference spectra of albumin (protein), dipalmitoyl-sn-glycero-3-phosphocholine (DPPC) (lipid), and alginic acid (polysaccharide) were recorded along the C K-edge (280–300 eV) (Figure S2). The uranium reference spectrum was collected along its $4d_{5/2}$ edges (720–780 eV), catching both peaks in that range (Figure S3). All the spectra were normalized to an optical density (OD) corresponding to a 1-nm layer. Uranium localization maps were obtained by subtracting the aligned below edge (725 eV) image from the above edge (738 eV) image. STXM data collection was conducted on the STXM end station 11.0.2.2 of the Molecular Environmental Science beam line 11.0.2 at the Advanced Light Source (ALS). Acquired image stacks were processed using the aXis 2000 software [54] package as previously described.

3.5. Bicarbonate Extraction Method

Extraction of non-crystalline U(IV) was performed by treating samples with anoxic 1.0 M sodium bicarbonate solution, pH 8.7. Cells were centrifuged for 10 min at 10,000 *g*. Supernatant was removed and centrifuged pellets were suspended in small volumes of BP medium to create concentrated stock cell slurry solutions. The slurries were diluted to OD_{600} = 1. To monitor non-crystalline U(IV) extraction kinetics, 1 mL samples were taken periodically and filtered through 0.2 μm membranes. Filtrate was diluted into 4.5 mL oxic 1.0 M HNO_3 and analyzed using inductively coupled plasma optical emission spectrometry (ICP-OES) to quantify extracted U [19].

4. Conclusions

In summary, we have uncovered a novel microbial strategy to combat encrustation resulting from metal reduction. Membrane vesicles, a phenomenon that has been often observed by electron microscopy, has been identified as a strategy to rid the cell of minerals encrusted on its surface. This finding provides an important clue to microbial approaches for dealing with uncontrolled biomineralization. This is a question that has been raised for decades but, in the case of metal-reducing bacteria, did not find a suitable explanation until now. EPS formation remains an additional strategy to MV formation. Based on our results, the two tacks appear to be unrelated as one or the other dominates depending on the circumstance. Future work should focus on the conditions that favor MV *vs.* EPS formation in the environment for the prevention of bacterial encrustation in minerals.

Acknowledgments

We acknowledge funding from the SLAC Science Focus Area funded by the U.S. DOE Subsurface Biogeochemical Research program (work package #10094). The Advanced Light Source is supported by the Director, Office of Science, Office of Basic Energy Sciences, of the U.S. Department of Energy under Contract No. DE-AC02-05CH11231. ALS-MES beamline 11.0.2 is supported by the Director, Office of Science, Office of Basic Energy Sciences, Division of Chemical Sciences, Geosciences, and Biosciences and Materials Sciences Division of the U.S. Department of Energy at the Lawrence Berkeley National Laboratory. Luis R. Comolli's work was supported by grant DOE-ERSP-ER65009 and by the Director, Office of Science, Office of Basic Energy Sciences, of the U.S. Department of Energy under Contract No. DE-AC02-05CH11231.

Conflict of Interest

The authors declare no conflict of interest.

References

1. Miot, J.; Benzerara, K.; Obst, M.; Kappler, A.; Hegler, F.; Schadler, S.; Bouchez, C.; Guyot, F.; Morin, G. Extracellular iron biomineralization by photoautotrophic iron-oxidizing bacteria. *Appl. Environ. Microb.* **2009**, *75*, 5586–5591.
2. Schadler, S.; Burkhardt, C.; Hegler, F.; Straub, K.L.; Miot, J.; Benzerara, K.; Kappler, A. Formation of cell-iron-mineral aggregates by phototrophic and nitrate-reducing anaerobic Fe(II)-oxidizing bacteria. *Geomicrobiol. J.* **2009**, *26*, 93–103.
3. Roden, E.E. Microbial iron-redox cycling in subsurface environments. *Biochem. Soc. Trans.* **2012**, *40*, 1249–1256.
4. Emerson, D.; Roden, E.; Twining, B.S. The microbial ferrous wheel: Iron cycling in terrestrial, freshwater, and marine environments. *Front. Microbiol.* **2012**, *3*, 383.
5. Gledhill, M.; Buck, K.N. The organic complexation of iron in the marine environment: A review. *Front. Microbiol.* **2012**, *3*, 69.
6. Tebo, B.M.; Johnson, H.A.; McCarthy, J.K.; Templeton, A.S. Geomicrobiology of manganese(II) oxidation. *Trends Microbiol.* **2005**, *13*, 421–428.
7. Spiro, T.G.; Bargar, J.R.; Sposito, G.; Tebo, B.M. Bacteriogenic manganese oxides. *Acc. Chem. Res.* **2010**, *43*, 2–9.
8. Lovley, D.R. *Environmental Microbe-Metal Interactions*; ASM: Washington, DC, USA, 2000.
9. Miot, J.; Maclellan, K.; Benzerara, K.; Boisset, N. Preservation of protein globules and peptidoglycan in the mineralized cell wall of nitrate-reducing, iron(II)-oxidizing bacteria: A cryo-electron microscopy study. *Geobiology* **2011**, *9*, 459–470.
10. Chan, C.S.; Fakra, S.C.; Edwards, D.C.; Emerson, D.; Banfield, J.F. Iron oxyhydroxide mineralization on microbial extracellular polysaccharides. *Geochim. Cosmochim. Acta* **2009**, *73*, 3807–3818.

11. Hegler, F.; Schmidt, C.; Schwarz, H.; Kappler, A. Does a low-pH microenvironment around phototrophic Fe(II)-oxidizing bacteria prevent cell encrustation by Fe(III) minerals? *Fems. Microbiol. Ecol.* **2010**, *74*, 592–600.
12. Beveridge, T.J. Role of cellular design in bacterial metal accumulation and mineralization. *Annu. Rev. Microbiol.* **1989**, *43*, 147–171.
13. Saini, G.; Chan, C.S. Near-neutral surface charge and hydrophilicity prevent mineral encrustation of Fe-oxidizing micro-organisms. *Geobiology* **2013**, *11*, 191–200.
14. Shelobolina, E.S.; Coppi, M.V.; Korenevsky, A.A.; DiDonato, L.N.; Sullivan, S.A.; Konishi, H.; Xu, H.; Leang, C.; Butler, J.E.; Kim, B.C.; *et al.* Importance of c-type cytochromes for U(VI) reduction by *Geobacter sulfurreducens*. *BMC Microbiol.* **2007**, *8*, 7–16.
15. Fredrickson, J.K.; Zachara, J.M.; Kennedy, D.W.; Liu, C.; Duff, M.C.; Hunter, D.B.; Dohnalkova, A. Influence of Mn oxides on the reduction of uranium(VI) by the metal-reducing bacterium *Shewanella putrefaciens*. *Geochim. Cosmochim. Acta* **2002**, *66*, 3247–3262.
16. Bernier-Latmani, R.; Veeramani, H.; Vecchia, E.D.; Junier, P.; Lezama-Pacheco, J.S.; Suvorova, E.I.; Sharp, J.O.; Wigginton, N.S.; Bargar, J.R. Non-uraninite products of microbial U(VI) reduction. *Environ. Sci. Technol.* **2010**, *44*, 9456–9462.
17. Bargar, J.R.; Williams, K.H.; Campbell, K.M.; Long, P.E.; Stubbs, J.E.; Suvorova, E.I.; Lezama-Pacheco, J.S.; Alessi, D.S.; Stylo, M.; Webb, S.M.; *et al.* Uranium redox transition pathways in acetate-amended sediments. *Proc. Natl. Acad. Sci. USA* **2013**, *110*, 4506–4511.
18. Kelly, S.D.; Kemner, K.M.; Carley, J.; Criddle, C.; Jardine, P.M.; Marsh, T.L.; Phillips, D.; Watson, D.; Wu, W.-M. Speciation of uranium in sediments before and after *in situ* biostimulation. *Environ. Sci. Technol.* **2008**, *42*, 1558–1564.
19. Alessi, D.S.; Uster, B.; Veeramani, H.; Suvorova, E.I.; Lezama-Pacheco, J.S.; Stubbs, J.E.; Bargar, J.R.; Bernier-Latmani, R. Quantitative separation of monomeric U(IV) from UO_2 in products of U(VI) reduction. *Environ. Sci. Technol.* **2012**, *46*, 6150–6157.
20. Shao, P.P.; Comolli, L.R.; Stylo, M.; Alessi, D.S.; Bargar, J.R.; Bernier-Latmani, R. Microbial extracellular polymeric substances modulate the product of uranium biomineralization. *Geobiology* **2013**, submitted.
21. Kulp, A.; Kuehn, M.J. Biological functions and biogenesis of secreted bacterial outer membrane vesicles. *Annu. Rev. Microbiol.* **2010**, *64*, 163–184.
22. Schwechheimer, C.; Sullivan, C.J.; Kuehn, M.J. Envelope control of outer membrane vesicle production in Gram-negative bacteria. *Biochemistry* **2013**, *52*, 3031–3040.
23. Beveridge, T.J. Structures of Gram-negative cell walls and their derived membrane vesicles. *J. Bacteriol.* **1999**, *181*, 4725–4733.
24. Inagaki, S.; Onishi, S.; Kuramitsu, H.K.; Sharma, A. *Porphyromonas gingivalis* vesicles enhance attachment, and the leucine-rich repeat BspA protein is required for invasion of epithelial cells by "*Tannerella forsythia*". *Infect. Immun.* **2006**, *74*, 5023–5028.
25. Grenier, D.; Mayrand, D. Functional characterization of extracellular vesicles produced by *Bacteroides gingivalis*. *Infect. Immun.* **1987**, *55*, 111–117.
26. Furuta, N.; Takeuchi, H.; Amano, A. Entry of *Porphyromonas gingivalis* outer membrane vesicles into epithelial cells causes cellular functional impairment. *Infect. Immun.* **2009**, *77*, 4761–4770.

27. Kesty, N.C.; Mason, K.M.; Reedy, M.; Miller, S.E.; Kuehn, M.J. Enterotoxigenic *Escherichia coli* vesicles target toxin delivery into mammalian cells. *EMBO J.* **2004**, *23*, 4538–4549.
28. Kolling, G.L.; Matthews, K.R. Export of virulence genes and shiga toxin by membrane vesicles of *Escherichia coli* O157:H7. *Appl. Environ. Microbiol.* **1999**, *65*, 1843–1848.
29. Kadurugamuwa, J.L.; Beveridge, T.J. Virulence factors are released from *Pseudomonas aeruginosa* in association with membrane vesicles during normal growth and exposure to gentamicin: A novel mechanism of enzyme secretion. *J. Bacteriol.* **1995**, *177*, 3998–4008.
30. Dubern, J.F.; Diggle, S.P. Quorum sensing by 2-alkyl-4-quinolones in *Pseudomonas aeruginosa* and other bacterial species. *Mol. Biosyst.* **2008**, *4*, 882–888.
31. Mashburn, L.M.; Whiteley, M. Membrane vesicles traffic signals and facilitate group activities in a prokaryote. *Nature* **2005**, *437*, 422–425.
32. Renelli, M.; Matias, V.; Lo, R.Y.; Beveridge, T.J. DNA-containing membrane vesicles of *Pseudomonas aeruginosa* Pao1 and their genetic transformation potential. *Microbiology* **2004**, *150*, 2161–2169.
33. Whitchurch, C.B.; Tolker-Nielsen, T.; Ragas, P.C.; Mattick, J.S. Extracellular DNA required for bacterial biofilm formation. *Science* **2002**, *295*, 1487.
34. Yonezawa, H.; Osaki, T.; Kurata, S.; Fukuda, M.; Kawakami, H.; Ochiai, K.; Hanawa, T.; Kamiya, S. Outer membrane vesicles of *Helicobacter pylori* TK1402 are involved in biofilm formation. *BMC Microbiol* **2009**, *9*, 197, doi:10.1186/1471-2180-9-197.
35. Schooling, S.R.; Beveridge, T.J. Membrane vesicles: An overlooked component of the matrices of biofilms. *J. Bacteriol.* **2006**, *188*, 5945–5957.
36. Tan, T.T.; Morgelin, M.; Forsgren, A.; Riesbeck, K. *Haemophilus influenzae* survival during complement-mediated attacks is promoted by *Moraxella catarrhalis* outer membrane vesicles. *J. Infect. Dis.* **2007**, *195*, 1661–1670.
37. Ciofu, O.; Beveridge, T.J.; Kadurugamuwa, J.; Walther-Rasmussen, J.; Hoiby, N. Chromosomal beta-lactamase is packaged into membrane vesicles and secreted from *Pseudomonas aeruginosa*. *J. Antimicrob. Chemother.* **2000**, *45*, 9–13.
38. McBroom, A.J.; Kuehn, M.J. Release of outer membrane vesicles by Gram-negative bacteria is a novel envelope stress response. *Mol. Microbiol.* **2007**, *63*, 545–558.
39. Tazaki, K.; Rafiqul, I.A.; Nagai, K.; Kurihara, T. $FeAs_2$ biomineralization on encrusted bacteria in hot springs: An ecological role of symbiotic bacteria. *Can. J. Earth Sci.* **2003**, *40*, 1725–1738.
40. Benzerara, K.; Morin, G.; Yoon, T.H.; Miot, J.; Tylisczcak, T.; Casiot, C.; Bruneel, O.; Farges, F.; Brown, G.E. Nanoscale study of as biomineralization in an acid mine drainage system. *Geochim. Cosmochim. Acta* **2008**, *72*, 3949–3963.
41. Aloisi, G.; Gloter, A.; Krueger, M.; Wallmann, K.; Guyot, F.; Zuddas, P. Nucleation of calcium carbonate on bacteria nanoglobules. *Geology* **2006**, *34*, 1017–1020.
42. Rakshe, S.; Leff, M.; Spormann, A.M. Indirect modulation of the intracellular c-Di-GMP level in *Shewanella oneidensis* MR-1 by MxdA. *Appl. Environ. Microb.* **2011**, *77*, 2196–2198.
43. Thormann, K.M.; Duttler, S.; Saville, R.M.; Hyodo, M.; Shukla, S.; Hayakawa, Y.; Spormann, A.M. Control of formation and cellular detachment from *Shewanella oneidensis* MR-1 biofilms by cyclic Di-GMP. *J. Bacteriol.* **2006**, *188*, 2681–2691.

44. Gorby, Y.; McLean, J.; Korenevsky, A.; Rosso, K.; El-Naggar, M.Y.; Beveridge, T.J. Redox-reactive membrane vesicles produced by *Shewanella*. *Geobiology* **2008**, *6*, 232–241.
45. Dohnalkova, A.C.; Marshall, M.J.; Arey, B.W.; Williams, K.H.; Buck, E.C.; Fredrickson, J.K. Imaging hydrated microbial extracellular polymers: Comparative analysis by electron microscopy. *Appl. Environ. Microb.* **2011**, *77*, 1254–1262.
46. Cologgi, D.L.; Lampa-Pastirk, S.; Speers, A.M.; Kelly, S.D.; Reguera, G. Extracellular reduction of uranium via *Geobacter* conductive pili as a protective cellular mechanism. *Proc. Natl. Acad. Sci. USA* **2011**, *108*, 15248–15252.
47. Bencheikh-Latmani, R.; Williams, S.M.; Haucke, L.; Criddle, C.S.; Wu, L.Y.; Zhou, J.Z.; Tebo, B.M. Global transcriptional profiling of *Shewanella oneidensis* MR-1 during Cr(VI) and U(VI) reduction. *Appl. Environ. Microb.* **2005**, *71*, 7453–7460.
48. Sokolov, I.; Smith, D.S.; Henderson, G.S.; Gorby, Y.A.; Ferris, F.G. Cell surface electrochemical heterogeneity of the Fe(III)-reducing bacteria *Shewanella putrefaciens*. *Environ. Sci. Technol.* **2001**, *35*, 341–347.
49. Liu, C.; Zachara, J.M.; Gorby, Y.A.; Szecsody, J.E.; Brown, C.F. Microbial reduction of Fe(III) and sorption/precipitation of Fe(II) on *Shewanella putrefaciens* strain CN32. *Environ. Sci. Technol.* **2001**, *35*, 1385–1393.
50. Studer, D.; Graber, W.; Al-Amoudi, A.; Eggli, P. A new approach for cryofixation by high-pressure freezing. *J. Microsc.* **2001**, *203*, 285–294.
51. The Boulder Lab for 3D Electron Microscopy of Cells. Available online: http://bio3d.colorado.edu/ (accessed on 26 January 2014).
52. Kremer, J.R.; Mastronarde, D.N.; McIntosh, J.R. Computer visualization of three-dimensional image data using imod. *J. Struct. Biol.* **1996**, *116*, 71–76.
53. ImageJ. Available online: http://rsb.info.nih.gov/ij/ (accessed on 26 January 2014).
54. aXis 2000—Analysis of X-ray Images and Spectra. Available online: http://unicorn.mcmaster.ca/aXis2000.html (accessed on 26 January 2014).